analytical chemistry

Article

pubs.acs.org/ac

Electrochemical Detection of Insulating Beads at Subattomolar Concentration via Magnetic Enrichment in a Microfluidic Device

Jason J. Yoo, Morgan J. Anderson, Timothy M. Alligrant, and Richard M. Crooks*

Department of Chemistry, Center for Electrochemistry, and the Center for Nano- and Molecular Science and Technology, The University of Texas at Austin, 105 East 24th Street Stop A5300, Austin, Texas 78712-1224, United States

Supporting Information

ABSTRACT: We report electrochemical detection of collisions between individual magnetic microbeads, present at subattomolar concentrations, and electrode surfaces. This limit of detection is 4 orders of magnitude lower than has been reported previously, and it is enabled by using a magnetic field to preconcentrate the microbeads prior to detection in a microfluidic electrochemical cell. Importantly, the frequency of collisions between the microbeads and the electrode is not compromised by the low concentration of microbeads. These findings represent an unusual case of detecting individual electrochemical events at very low analyte concentration. In addition to experiments supporting these claims, finite-element simulations provide additional insights into the nature of the interactions between flowing microbeads and their influence on electrochemical processes.

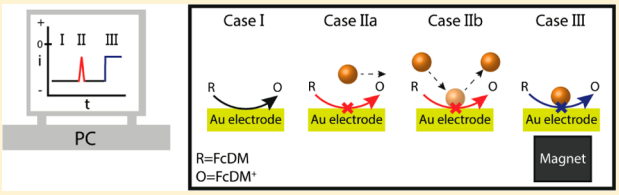

Here, we report electrochemical detection of individual particles present in solution at subattomolar concentrations, which is 4 orders of magnitude lower than previously attained. Importantly, despite this low limit of detection, the detection frequency is not compromised. As shown in Scheme 1a, microbeads are detected when they approach an electrode surface and partially block mass transfer of an electroactive redox probe molecule. The low detection threshold and relatively high detection frequency are achieved by manipulating a permanent magnet, which slides along the length of the microfluidic channel, to enrich the insulating microbeads and thereby concentrate them at the electrode surface. This approach addresses a long-standing problem in the field of microfluidics: coupling single-particle detection with highly dilute analyte solutions. It is likely that this same general strategy can be used to detect individual biomolecules present at low concentration and linked to magnetic beads.

The results reported here build upon the pioneering studies of Lemay and co-workers, who reported the first example of electrochemical detection of individual microbeads ten years ago.[1] In their experiment, 150 and 500 nm latex beads collided with, and irreversibly adsorbed to, the surface of a 2.5 μm Au ultramicroelectrode (UME). Each adsorption event led to a stepwise decrease in the faradaic current arising from partially blocked mass transport of a redox probe (ferrocenemethanol, FcMeOH) to the electrode surface. Importantly, the collision frequency increased as the electrolyte concentration decreased because of electromigration of the negatively charged beads.

Bard and co-workers extended Lemay's findings and were able to detect microbead concentrations as low as 5 fM but only at very low electrolyte concentration (1 mM KCl).[2] On the basis of finite element simulations, they predicted a correlation between the amplitude of the current blocking events and the location of the collision on the UME. Subsequently, our group confirmed their predictions experimentally using simultaneous amperometric detection and optical tracking, and we provided additional insights into the nature of collisions between beads and electrodes.[3] In addition to the foregoing collision experiments involving insulating beads and electrode surfaces, there have been a large number of reports from the following groups involving collisions between catalytic nanoparticles and electrodes: Bard,[4−12] Stevenson,[13] Compton,[14−16] Koper,[17] Unwin,[18] Alpuche-Aviles,[19] and Crooks.[20] The range of nanoparticle and microbead concentrations detected in these experiments was 50 fM−700 pM. Collision frequencies were found to vary linearly with concentration and ranged from 0.01 to 0.04 $s^{-1}pM^{-1}$ of particle concentration.

There have been several examples of magnets being integrated with microfluidic systems with the goal of lowering detection limits. For example, Verbarg et al. used a spinning permanent magnetic trap to capture, mix, and release target molecules using magnetic beads within a microfluidic channel.[21] In this experiment, six pairs of permanent magnets were affixed to a rotating wheel located underneath the channel. As the wheel rotated in the opposite direction of fluidic flow, the magnetic beads were briefly concentrated until the magnet rotated away, freeing the beads until the rotating magnet once again entrapped them. Permanent magnets have also been used to detect nucleic acid sequences,[22] perform immunoassays,[23] capture magnetic beads,[24−26] and change the direction of flow of magnetic particles or droplets for purposes of separation.[27,28] By incorporating more sophisticated microfluidic fabrication

Received: December 17, 2013
Accepted: April 4, 2014
Published: April 18, 2014

Scheme 1

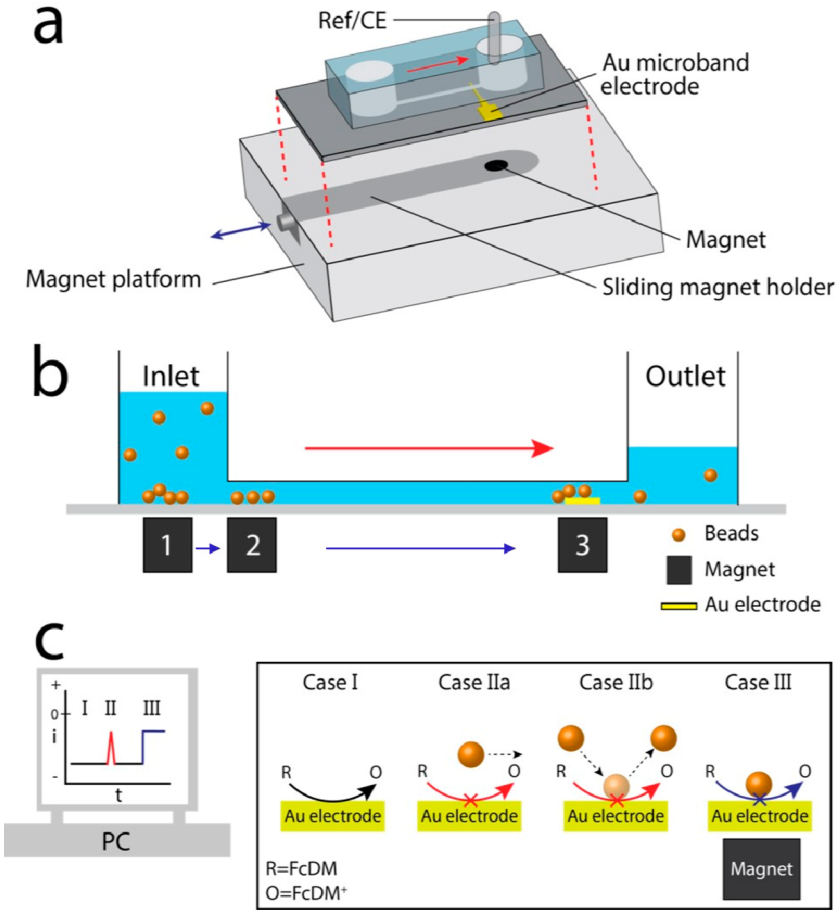

processes, electromagnets have also been utilized to isolate and capture target molecules.[29,30]

EXPERIMENTAL SECTION

Chemicals. Sodium phosphate monobasic monohydrate (phosphate, 100%) polysorbate 20 (Tween 20, 100%), and acetone (99.9%) were purchased from Fisher Scientific (Fair Lawn, NJ) and used as received. 1,1′-Ferrocenedimethanol (FcDM, 98%) was purchased from Sigma-Aldrich (St. Louis, MO) and ethanol (99.5%) was purchased from Pharmco-AAPER (Shelbyville, KY). Deionized water (DI water, 18.2 MΩ-cm) was used for all experiments and was obtained from a Millipore filtration system (Millipore, Bedford, MA).

The solution used for electrochemical experiments was prepared as follows. First, 5.0 mM FcDM and 50 mM pH 7.0 phosphate buffer in DI water were mixed. Second, 0.1% volume of the surfactant Tween 20 was added to the solution followed by sonication for 20 min. Tween 20 was used to prevent bead aggregation. Third, the sonicated solution was filtered through a vented Millex-GS 0.22 μm syringe filter unit attached to a LUER-Slip plastic syringe. In some cases magnetic COMPEL COOH-functionalized fluorescent beads (2.82 μm diameter, inventory number: L110121A, Bangs Laboratories, Inc., Fishers, IN) were added to the solution.

Fluidics. The configuration of the fluidic device used in the present study is illustrated in Scheme 1a. The fluidic channel, 3 mm (l) × 27 μm (w) × 19 μm (h), was cast in poly(dimethylsiloxane) (PDMS) using standard micromolding techniques.[31] Inlet and outlet reservoirs (4 mm diameter) were punched through the PDMS. The base of the fluidic channel consisted of a glass slide, onto which a 17 μm × 27 μm Au electrode had been microfabricated. The PDMS monolith and glass base were then bound together, and the resulting microelectrochemical cell was attached to the plastic magnet holder. To control the solution flow direction (red arrows in Schemes 1a and 1b) and rate within the microchannel, the inlet and outlet were filled with 40 and 15 μL, respectively, of a solution containing 5.0 mM ferrocenedimethanol (FcDM), 0.1% Tween 20, and 50 mM pH 7.0 phosphate buffer. Finally, a small Ag/AgCl leakless reference electrode was placed in the outlet reservoir and used as both the reference (ref) and counter (CE) electrodes in a two-electrode configuration. Additional information about the fabrication methods, and step-by-step photographs of the assembly process, are provided in the Supporting Information.

Electrochemistry. Cyclic voltammetry (CV) and *i*−*t* curves were obtained using a Chem-Clamp voltammeter-amperometer (Dagan Corp., Minneapolis, MN) and a PAR 175 Universal Function Generator (Princeton Applied Research, Oak Ridge, TN). Both the potentiostat and the generator were connected to a Dell Optiplex 380 computer through a PCI-6251 data acquisition board using a BNC-2090A analog breakout accessory (National Instruments, Austin, TX). The CV and *i*−*t* data were translated using a custom program written in LabView 2010 (National Instruments). The sampling time for all experiments was 0.025 s unless otherwise stated. Electrochemical measurements were obtained using a Faraday cage constructed from copper plate and mesh. For optical tracking

dx.doi.org/10.1021/ac404093c | Anal. Chem. 2014, 86, 4302−4307

experiments, a Faraday cage was constructed using a cardboard box wrapped in aluminum foil. A hole the size of the microscope objective was cut into the top of the box. All potentials reported in this paper were referenced to a Ag/AgCl "leakless" reference electrode (Dionex, 3.4 M KCl, model 66-EE009 "Leakless", Bannockburn, IL).

Numerical Simulations. Finite-element simulations were performed using a Dell Precision T7500 workstation equipped with Dual Six Core Intel Xeon Processors (2.40 GHz) and 24 GB of RAM. Simulations were performed using the COMSOL Multiphysics version 4.3 commercial package. All simulations were performed at steady state. Additional details about the simulations are provided in the Supporting Information.

RESULTS AND DISCUSSION

Fluidics. The microelectrochemical cell used in the present study is illustrated in Scheme 1a and described in detail in the Experimental Section and the Supporting Information. Briefly, however, the fluidic channel, 3 mm (l) × 27 μm (w) × 19 μm (h), was cast in PDMS. This monolith was then attached to a glass slide supporting a 17 μm × 27 μm Au working electrode. The direction and rate of fluid flow was controlled using differential heights of solution in the inlet and outlet reservoirs (Scheme 1b).

Electrochemistry. Figure 1a presents $i-t$ curves for flowing FcDM measured for 5 min at a mass-transfer-limited oxidizing potential of 450 mV vs Ag/AgCl (Supporting Information Figure S2a) under different experimental conditions. The black trace, which corresponds to Case I in Scheme 1c, is a background $i-t$ curve obtained in the absence of microbeads. A slowly decreasing anodic current of about −32 nA is observed. This limiting current (i_L) varied by ±3 nA from device to device, likely because of slight differences in channel dimensions and relative solution heights, which influences the flow rate (Scheme 1b). The small decrease in i_L over time observed in some $i-t$ curves may be due to the adsorption of trace contaminants or a gradual decrease in flow rate within the channel due to the small time-dependent change in the levels of solution in the reservoirs.

After recording the background $i-t$ curve, the solution in the inlet reservoir was removed and replaced with the same volume of the FcDM solution, but now containing 30 aM microbeads. The resulting red $i-t$ trace in Figure 1a reveals two small, short-duration current peaks at t = 33 (see inset) and 265 s. We believe this type of peak-shaped feature is due to microbeads in sufficiently close proximity to the working electrode that mass transfer of FcDM is hindered (Case IIa in Scheme 1c). However, fluorescence microscopy reveals that not every bead passing over the electrode results in a current transient. Indeed, the beads that yielded electrochemical signatures had slower linear velocities than those that did not (Supporting Information Figures S3 and S4 and Movie S1). A possible explanation is that the slower microbeads are lower in the parabolic laminar flow profile, meaning they are close to the electrode and hence have a detectable effect on mass transfer of FcDM. In contrast, faster moving microbeads in more central flow laminas do not perturb the diffusion layer to the same degree or are moving too fast for the recording equipment to detect their passage from the background noise (33 pA, see discussion in Supporting Information). Another possible scenario for these peak-shaped transients involves the bead striking the electrode and then continuing downstream (Case IIb in Scheme 1c). Although the red trace in Figure 1a reveals

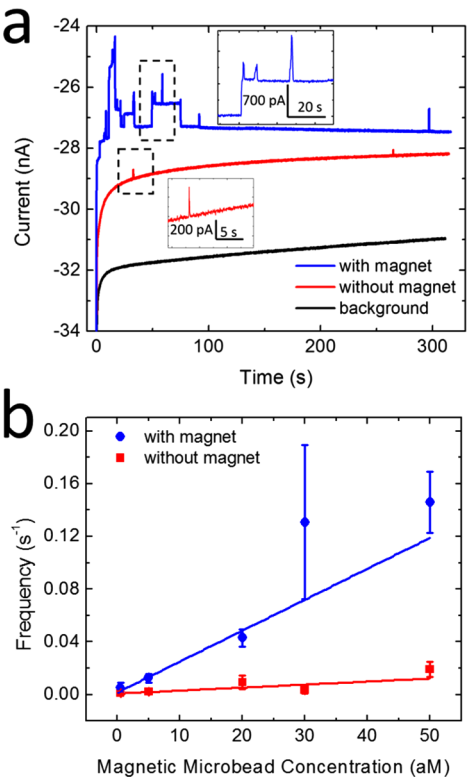

Figure 1. (a) Chronoamperometric curves recorded in the absence (black trace) and presence (blue and red traces) of 30 aM magnetic microbeads. The red and blue curves were obtained in the absence and presence, respectively, of a magnetic field. The insets show an expanded view of the indicated portions of the $i-t$ curves. (b) Plot of the frequency of current transients (both steps and peaks) as a function of the concentration of magnetic microbeads in the absence (red line) and presence (blue line) of a magnetic field. The error bars represent the standard deviation of signals collected from >3 independent experiments. For all experiments the solution contained 5.0 mM FcDM, 50 mM phosphate buffer (pH 7), and 0.1% Tween 20. The nominal dimensions of the Au microband working electrode were 27 μm × 17 μm, and it was held at a potential of 450 mV vs Ag/AgCl.

only peak-shaped current features, 21% of such features were longer-lasting and step shaped. The average frequency of the current transients (combined peaks and steps) was 0.0037 s^{-1}.

Magnetic Enrichment. Magnetic field-induced bead enrichment was carried out using the approach illustrated in Scheme 1b. Here, the small burnt orange circles represent the beads, the large black squares represent the magnet present at different locations along the microchannel, and the small yellow rectangle is the Au microband electrode. The red arrow shows the direction of solution flow.

The enrichment steps concentrate the beads inside the channel, thereby increasing the probability of detection at the Au microband electrode. During the first enrichment step, the magnet is positioned beneath the inlet for 5 min to draw the microbeads to the bottom of the inlet. Next, the magnet is aligned with the entrance of the channel for 5 min, thereby assisting transfer of the beads from the inlet to the channel. Finally, the magnet is positioned under the working Au microband electrode for an additional 5 min, and it is during this time period that the $i-t$ data represented by the blue trace in Figure 1a was recorded. Note that cylindrical neodymium permanent magnet (grade = N48) is much larger in diameter (1.6 mm) than the working electrode (17 μm × 27 μm), which

dx.doi.org/10.1021/ac404093c | Anal. Chem. 2014, 86, 4302−4307

means it is important to reproducibly align the magnet with the electrode in each experiment. The beads respond to the external magnetic field during each of the three enrichment steps, but the number of beads enriched at each step is progressively reduced because not all of them respond to the magnetic field within the allotted enrichment time and some adhere to the walls of the microchannel.

The blue trace in Figure 1a is the $i-t$ curve obtained for 30 aM beads in the presence of the magnet using the three just-discussed enrichment steps. Compared to the red trace (no magnet), the total number of current transients (both steps and peaks) increases markedly and the ratio of current steps to current peaks also increases from 21% in the absence of the magnet to 42% in its presence. The latter observation can be attributed to the magnetic field concentrating the beads at the electrode surface, thereby causing them to irreversibly adhere (Case III in Scheme 1c). However, the current sometimes returns to the background value (e.g., t = ~30−50 s), and optical observations indicate that this occurs when one bead knocks the adsorbed bead(s) off the electrode thereby exposing the once-blocked surface. Also, the experiment shows that most of the beads adhere to the leading edge of the electrode (Supporting Information Movie S2). At a bead concentration of 30 aM, the average frequency of current excursions in the presence of the magnet is 0.13 s^{-1}. Figure 1b is a plot of collision frequency vs microbead concentration spanning the range 0.5−50 aM (the original data from which Figure 1b is extracted are provided in Supporting Information Figure S2). There is a roughly linear relationship between the frequency of current excursions and microbead concentration both in the presence (2.35×10^3 $s^{-1}pM^{-1}$, R^2 = 0.94) and the absence (2.28×10^2 $s^{-1}pM^{-1}$, R^2 =0.98) of the magnet, though there is a significant positive deviation from this trend at higher concentrations in the presence of the magnetic field.

Interestingly, these frequencies are two to 4 orders of magnitude higher than previously reported (0.01−11 s^{-1} pM^{-1}).[1−20] We attribute the higher flux in the present work to the size of the microbeads (2.82 μm) in relation to the microchannel and microelectrode dimensions (27 μm × 19 μm and 17 μm × 27 μm, respectively). For example, the 2.82 μm microbeads account for ~15% of the channel height, and unlike nanometer-scale particles they need only approach the electrode to influence the flux of FcDM.

Figure 2a is a histogram of the normalized distribution of magnitudes ($-i_T/i_L$) of the peaked (black) and stepped (red) current excursions, where i_T is the signal intensity of the current transients (peaks or steps) and i_L is the limiting current. For the peaked signals, the distribution of $-i_T/i_L$ values does not exhibit a clear pattern, though there is a general trend toward lower frequencies for larger normalized current excursions. However, for the step-shaped signals, a distinct pattern, which looks like a Poisson distribution, does emerge.

Numerical Simulations. To better understand the foregoing experimental results, we carried out finite-element simulations using the COMSOL Multiphysics version 4.3 software package. However, we could only simulate the stepped features, as it was not possible to simulate the peaked feature with our current modeling capabilities. The channel geometry (Figure 2b) used was identical to the nominal geometry used in the experiments, though there was minor device-to-device variation in both electrode area and channel dimensions. Because of symmetry, the channel was halved with the channel wall at the top of Figure 2b and the axial center line of the channel at the bottom (y coordinate = 0). The flow is from left to right as the arrows indicate. An array of spheres (orange circles in Figure 2b) was positioned near the electrode surface, and then the spheres were systematically deactivated from the

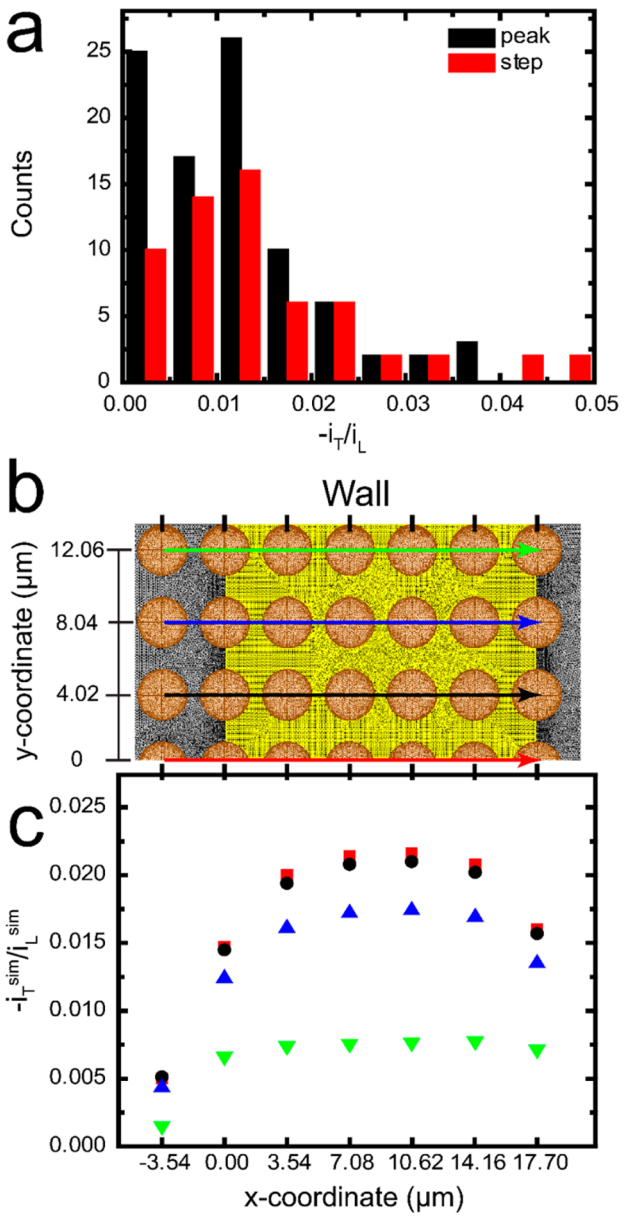

Figure 2. (a) Histogram showing the normalized distribution of current transients (steps and peaks) resulting from. The signal intensity of the current steps and peaks (i_T) is divided by the limiting current (i_L) to account for slight differences in the geometry of the independently prepared microelectrochemical devices used to acquire these data. (b) A top-down view illustrating the position of the spherical microbeads (shown as orange circles) relative to the electrode (shown in yellow) used for the finite-element simulations. The channel wall is at the top of the figure and the plane of symmetry is at the bottom. The direction of solution flow is from left to right. The coordinates show the relative position of the microbeads assuming that the plane of symmetry is located at y = 0 and the leading edge of the electrode is at x = 0. (c) Results of finite-element simulations. Each data point represents a sphere placed on the electrode surface. The coordinates of the data points corresponds to the center of the microbeads in panel b. The color of the data points corresponds to the color of the arrows in panel b.

dx.doi.org/10.1021/ac404093c | Anal. Chem. 2014, 86, 4302−4307

model to simulate insulating volumes (microbeads) at various locations on the channel floor. Finally, the Navier–Stokes and mass transport equations were solved to determine the current decrease from the insulating volumes.

The value of the simulated limiting current (i_L^{sim}) in the absence of beads was found to be −35 nA, which is comparable to the value of −32 nA shown in Figure 1a. The simulated step currents (i_T^{sim}) were calculated by subtracting the limiting current in the presence of the beads ($i_{L,bead}^{sim}$) from i_L^{sim}. Figure 2c shows the values of $-i_T^{sim}/i_L^{sim}$ as a function of the x-coordinate of each bead in Figure 2b. The colors of the symbols in Figure 2c are keyed to the corresponding colors of the arrows in Figure 2b. The simulation shows the highest values of $-i_T^{sim}/i_L^{sim}$ are toward the center of the channel (y = 0 in Figure 2b and black squares in Figure 2c), which is expected because this is the location of highest linear flow and hence highest current.[32]

The experimental results in Figure 2a showed that the largest number of steps were in the range of $-i_T/i_L$ values between 0.0075 and 0.015 (51%, Figure 2a).This range corresponds to the leading edge of the electrode in the simulations (Figures 2b): $-i_T^{sim}/i_L^{sim}$ = 0.005 to 0.015 at x = 0 in Figure 1c. Note that fluorescence tracking experiments show that most of the beads that stick to the electrode adhere to its leading edge (Supporting Information Movie S2). Full details of the simulation method and complete results are provided in the Supporting Information.

SUMMARY AND CONCLUSIONS

We have shown that microfluidics, electrochemistry, and magnetic preconcentration can be combined to detect individual collisions and near-collisions between microbeads and an electrode surface at concentrations as low as 500 zM. Importantly, magnetic preconcentration makes it possible to observe these collision events at reasonable frequencies. This result is important, because it resolves a general problem in analytical chemistry: that it is difficult to detect single events in solutions containing low analyte concentrations.[4,5,7−9] The results of the electrochemical experiments were supported with simulations and fluorescence microscopy, which provide additional insights into the nature of collisions between microbeads and the electrode surface. Specifically, the relationship between the location of the beads on the electrode and signal intensity under flowing conditions. The optical measurements also demonstrated that peak-shaped current transients correlate to beads traveling over the electrode but not adhering to it, while current steps arise from adherent microbeads.

There are some advantages of this experiment compared to previously reported particle detection methods.[1,2,4−10,13] First, permanent magnets are cheap, easy to use, and do not require additional instrumentation after fabrication. Second, the device design allows greater freedom of enrichment, compared to electromagnets, as the magnet can be easily moved to different locations.[33,34] Third, compared to previously reported results for electrochemical collision experiments, the approach described here allows detection of microbead concentrations 4 orders of magnitude lower in a shorter observation time: 500 zM and 300 s vs 5 fM and 5000 s.[2] Finally, the use of a magnetic field for preconcentration makes it possible to observe single-particle collisions under biologically relevant conditions (i.e., physiological electrolyte concentrations). This was not possible previously, because detection limits were enhanced by taking advantage of electrophoresis at electrolyte concentrations in the range of 0.5−5 mM. This will be important in our forthcoming reports of detection of individual biomolecules present at low concentration, which will be reported in due course.

ASSOCIATED CONTENT

Supporting Information

Information about chemicals, materials, procedures, and fabrication of the microelectrochemical cell, a cyclic voltammogram and i−t curves obtained for different concentrations of magnetic microbeads, histogram showing the linear velocity of the flowing magnetic microbeads, a movie showing microbeads moving in the microchannel and a corresponding i−t curve, SEM image, size-distribution histogram for the magnetic microbeads, and information about the numerical simulations. This material is available free of charge via the Internet at http://pubs.acs.org.

AUTHOR INFORMATION

Corresponding Author

*. E-mail: crooks@cm.utexas.edu. Voice: 512-475-8674.

Notes

The authors declare no competing financial interest.

ACKNOWLEDGMENTS

We gratefully acknowledge financial support from the U.S. Defense Threat Reduction Agency (Grant No. HDTRA1-11-1-0005). The Robert A. Welch Foundation (Grant F-0032) provides sustained support for our research. We thank Prof. Allen J. Bard, Prof. Keith J. Stevenson (UT Austin) and Prof. Bo Zhang (University of Washington) for helpful discussions. We also thank Elizabeth G. Nettleton who carried out some preliminary experiments related to those described herein.

REFERENCES

(1) Quinn, B. M.; van't Hof, P. G.; Lemay, S. G. *J. Am. Chem. Soc.* **2004**, *126*, 8360−8361.
(2) Boika, A.; Thorgaard, S. N.; Bard, A. J. *J. Phys. Chem. B* **2013**, *117*, 4371−4380.
(3) Fosdick, S. E.; Anderson, M. J.; Nettleton, E. G.; Crooks, R. M. *J. Am. Chem. Soc.* **2013**, *135*, 5994−5997.
(4) Xiao, X.; Bard, A. J. *J. Am. Chem. Soc.* **2007**, *129*, 9610−9612.
(5) Xiao, X.; Fan, F.-R. F.; Zhou, J.; Bard, A. J. *J. Am. Chem. Soc.* **2008**, *130*, 16669−16677.
(6) Xiao, X.; Pan, S.; Jang, J. S.; Fan, F.-R. F.; Bard, A. J. *J. Phys. Chem. C* **2009**, *113*, 14978−14982.
(7) Bard, A. J.; Zhou, H.; Kwon, S. J. *Isr. J. Chem.* **2010**, *50*, 267−276.
(8) Zhou, H.; Fan, F.-R. F.; Bard, A. J. *J. Phys. Chem. Lett.* **2010**, *1*, 2671−2674.
(9) Park, J. H.; Boika, A.; Park, H. S.; Lee, H. C.; Bard, A. J. *J. Phys. Chem. C* **2013**, *117*, 6651−6657.
(10) Park, J. H.; Thorgaard, S. N.; Zhang, B.; Bard, A. J. *J. Am. Chem. Soc.* **2013**, *135*, 5258−5261.
(11) Kwon, S. J.; Bard, A. J. *J. Am. Chem. Soc.* **2012**, *134*, 10777−10779.
(12) Zhou, H.; Park, J. H.; Fan, F. −R. F.; Bard, A. J. *J. Am. Chem. Soc.* **2012**, *134*, 13212−13215.
(13) Dasari, R.; Robinson, D. A.; Stevenson, K. J. *J. Am. Chem. Soc.* **2013**, *135*, 570−573.
(14) Zhou, Y.-G.; Rees, N. V.; Compton, R. G. *Angew. Chem., Int. Ed.* **2011**, *50*, 4219−4221.
(15) Rees, N. V.; Zhou, Y.-G.; Compton, R. G. *RSC Adv.* **2012**, *2*, 379−384.
(16) Zhou, Y. G.; Rees, N. V.; Compton, R. G. *Chem. Commun.* **2012**, *48*, 2510−2512.

(17) Kleijn, S. E. F.; Serrano-Bou, B.; Yanson, A. I.; Koper, M. T. M. *Langmuir* **2013**, *29*, 2054−2064.
(18) Kleijn, S. E. F.; Lai, S. C. S.; Miller, T. S.; Yanson, A. I.; Koper, M. T. M.; Unwin, P. R. *J. Am. Chem. Soc.* **2012**, *134*, 18558−18561.
(19) Fernando, A.; Parajuli, S.; Alpuche-Aviles, M. A. *J. Am. Chem. Soc.* **2013**, *135*, 10894−10897.
(20) Alligrant, T. M.; Nettleton, E. G.; Crooks, R. M. *Lab Chip* **2013**, *13*, 349−354.
(21) Verbarg, J.; Kamgar-Parsi, K.; Shields, A. R.; Howell, P. B. J.; Ligler, F. S. *Lab Chip* **2012**, *12*, 1793−1799.
(22) Kwakye, S.; Baeumner, A. *Anal. Bioanal. Chem.* **2003**, *376*, 1062−1068.
(23) Choi, K.; Ng, A. H. C.; Fobel, R.; Chang-Yen, D. A.; Yarnell, L. E.; Pearson, E. L.; Oleksak, C. M.; Fischer, A. T.; Luoma, R. P.; Robinson, J. M.; Audet, J.; Wheeler, A. R. *Anal. Chem.* **2013**, *85*, 9638−9646.
(24) Fan, Z. H.; Mangru, S.; Granzow, R.; Heaney, P.; Ho, W.; Dong, Q.; Kumar, R. *Anal. Chem.* **1999**, *71*, 4851−4859.
(25) Berti, F.; Laschi, S.; Palchetti, I.; Rossier, J. S.; Reymond, F.; Mascini, M.; Marrazza, G. *Talanta* **2009**, *77*, 971−978.
(26) Ramadan, Q.; Gijs, M. A. M. *Procedia Chem.* **2009**, 1499−1502.
(27) Forbes, T. P.; Forry, S. P. *Lab Chip* **2012**, *12*, 1471−1479.
(28) Zhang, K.; Liang, Q.; Ma, S.; Mu, X.; Hu, P.; Wang, Y.; Luo, G. *Lab Chip* **2009**, *9*, 2992−2999.
(29) Kang, J. H.; Krause, S.; Tobin, H.; Mammoto, A.; Kanaphathipillai, M.; Ingber, D. E. *Lab Chip* **2012**, *12*, 2175−2181.
(30) Afshar, R.; Moser, Y.; Lehnert, T.; Gijs, M. A. M. *Sens. Actuators, B* **2011**, *154*, 73−80.
(31) Xia, Y.; Whitesides, G. M. *Annu. Rev. Mater. Sci.* **1998**, *28*, 153−184.
(32) Shah, R. K.; London, A. L. Laminar Flow Forced Convection in Ducts: A Source for Compact Heat Exchanger Analytical Data. *Advances in Heat Transfer*; Thomas, J., Irvine, F., Hartnett, J. P., Eds.; Academic Press: New York, 1978; Vol. Supplement *1*.
(33) Lee, C. S.; Lee, H.; Westervelt, R. M. *Appl. Phys. Lett.* **2001**, *79*, 3308−3310.
(34) Basore, J. R.; Lavrik, N. V.; Baker, L. A. *Langmuir* **2010**, *26*, 19239−19244.

NOTE ADDED AFTER ASAP PUBLICATION

This paper was published ASAP on April 18, 2014, with an error in the value of the linear relationship of the frequency of currents excursions and microbead concentration in the presence of the magnet in the text describing Figure 1b. The corrected manuscript was reposted on April 21, 2014.